SANDIA REPORT

SAND2001-0076
Unlimited Release
Printed March 2001

Dynamic Multi-Rigid-Body Systems with Concurrent Distributed Contacts: Theory and Examples*

Jeffrey C. Trinkle, J. A. Tzitzouris, J. S. Pang

Prepared by
Sandia National Laboratories
Albuquerque, New Mexico 87185 and Livermore, California 94550

Sandia is a multiprogram laboratory operated by Sandia Corporation,
a Lockheed Martin Company, for the United States Department of Energy under Contract DE-AC04-94AL85000.

Issued by Sandia National Laboratories, operated for the United States Department of Energy by Sandia Corporation.

Available to DOE and DOE contractors from
U.S. Department of Energy
Office of Scientific and Technical Information
P.O. Box 62
Oak Ridge, TN 37831

Telephone: (865)576-8401
Facsimile: (865)576-5728
E-Mail: reports@adonis.osti.gov
Online ordering: http://www.doe.gov/bridge

Available to the public from
U.S. Department of Commerce
National Technical Information Service
5285 Port Royal Rd
Springfield, VA 22161

Telephone: (800)553-6847
Facsimile: (703)605-6900
E-Mail: orders@ntis.fedworld.gov
Online order: http://www.ntis.gov/ordering.htm

SAND2001-0076
Unlimited Release
Printed March 2001

Dynamic Multi-Rigid-Body Systems with Concurrent Distributed Contacts: Theory and Examples *

Jeffrey C. Trinkle†
Intelligent Systems Principles Department
Sandia National Laboratories
P.O. Box 5800
Albuquerque, NM 87185-1004
Email: jctrink@sandia.gov

J. A. Tzitzouris
Department of Mathematical Sciences
The Johns Hopkins University
Baltimore, MD 21218-2689
Email: jimt2@mts.jhu.edu

J. S. Pang‡
Department of Mathematical Sciences
The Johns Hopkins University
Baltimore, MD f21218-2689
Email: jsp@vicp1.mts.jhu.edu

ABSTRACT

Consider a system of rigid bodies with multiple concurrent contacts. The multi-rigid-body contact problem is to predict the accelerations of the bodies and the normal friction loads acting at the contacts. This paper presents theoretical results for the multi-rigid-body contact problem under the assumptions that one or more contacts occur over locally planar, finite regions and that friction forces are consistent with the maximum work inequality. Existence and uniqueness results are presented for this problem under mild assumptions on the system inputs. In addition, the performance of two different time-stepping methods for integrating the dynamics are compared on two simple multi-body systems.

Key Words. Multi-rigid-body contact problem, torsional friction, maximum work inequality, complementarity, time-stepping methods.

---

*Any findings, conclusions, or recommendations expressed herein are those of the authors and do not necessarily reflect the views of the funding agencies. The technical portion of this paper is based on a paper presented in [14].

†Partially supported by the National Science Foundation under grant IRI-9619850, by the Texas Advanced Research Program grant 999903-078, by the Texas Advanced Technology Program under grant 999903-095, and Sandia National Laboratories. Sandia is a multi-program laboratory operated by Sandia Corporation, a Lockheed Martin Company, for the United States Department of Energy under Contract DE-AC04-94AL85000.

‡The research of this author was based on work supported by the National Science Foundation under grant IRI-9713034.

1 Introduction

Multi-body dynamic systems are ubiquitous in our society: motors, engines, and the automation devices used to build portions of these machines are common examples. Where possible, machine designers use joints that provide bilateral kinematic constraints between the connected bodies (*e.g.*, pin joints). Such joints are desired, because they are easy to analyze during design, and they have long operational lives. In some situations, however, design constraints dictate the use of "joints" which provide only unilateral kinematic constraint. For example, in the domain of automated manufacturing, parts feeders typically have rigid protrusions that interact with parts as they stream by. The protrusions reorient parts, but occasionally jam (see Figure 1.) In assembly applications, fixtures are designed to

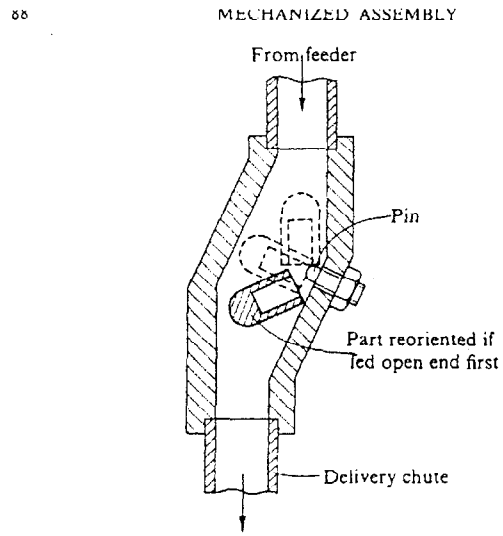

Figure 1: The exit orientation of the cup-shaped part must be with the curved portion down, regardless of the entering orientation [1].

hold parts in precise positions and orientations relative to each other and a reference frame. If a part comes to rest undetected before fully engaging the fixture, subsequent operations on the fixtured parts may not meet design specifications and may not be recognized until the completed product fails an inspection test.

Well-designed parts-feeding systems can save a significant portion of operating costs, while increasing quality and throughput. However, due to a lack of general, efficient software packages for simulating and analyzing systems with unilateral contacts[1], current design methods are error prone and inefficient. Further, when a design fails, there is no way to analyze it to determine if a simple modification could correct the problem.

This paper represents a step toward the development of improved engineering design tools for mechanical systems with unilateral contact. Following in the footsteps of Lötstedt and others who have popularized the use of complementarity methods in rigid body dynamics [7, 8, 11], we extend the model developed formally in [15] to include a frictional moment (transmitted about the contact normal). While it is not possible to transmit such a moment through a point contact (as would occur generically between curved rigid bodies), we include it in our model in recognition of the fact that contacts between stiff real bodies are distributed over small patches [6] and that the friction forces obey the maximum work inequality [5]. While in principle, the geometries of the contact patches could be arbitrary, the supporting empirical data presented in [6] and the leveraged theory in [5] assumed that contact patches were planar. Thus we include that assumption here.

The main contribution of this paper is a set of new existence and uniqueness results that provide strict theoretical guidelines for the use of our model in the analysis of multi-rigid-body dynamic systems with multiple distributed unilateral contacts. A secondary contribution is the demonstration that time-stepping methods can be used to accurately simulate such systems.

2 The Model

The derivation of our mathematical model describing the motion of a system of rigid bodies with locally planar, finite areas of contact is analogous to the model with isolated point contacts developed previously [15]. Therefore, in this paper, we will only detail the extension to include frictional moments in the directions of the contact normals at the distributed contacts. Our model consists of several sets of equations and inequalities enforcing the Newton-Euler equations of motion, kinematic nonpenetration constraints, and a dry friction law satisfying the maximum work inequality. When formulated at the current time, the solution to these equations and inequalities yields the accelerations of the bodies, the contact forces and moments, and the qualitative contact changes (e.g., contact separation

[1] Adams, DADS, Solid Works, and Working Model are some of the best available software packages, but they all have shortcomings in terms of generality and in identifying situations where the rigid body assumption leads to nonuniqueness.

or conversion from rolling to sliding). Integration of the accelerations over time yields the motion of the system.

We begin by assuming that there are a number of rigid bodies, each composed of a finite number of features (e.g., surface patches, edges between the patches, and vertices formed by the intersections of edges). The positions and orientations of the bodies are represented by the tuple $\boldsymbol{q}$. Given a feature on each of two bodies, one can derive a distance function $\psi_n(\boldsymbol{q})$ that is positive when the two features are separated, equal to zero when the two features are in contact, and negative when the two features interpenetrate. The nonpenetration constraint on the i^{th} feature pair is thus:

$$\psi_{in} \geq 0, \quad \forall\, i = 1, \ldots, n_c,$$

where n_c is the number of contact points. Since the dynamic equations are expressed in terms of accelerations, a contact is assumed to exist only if $\psi_{in} = 0$ and the normal component of relative velocity, $v_{in} = (\nabla_q \psi_{in})^T \dot{\boldsymbol{q}} = 0$, where $\nabla_q \psi_{in}$ is the gradient of ψ_{in} with respect to the configuration variable, $\boldsymbol{q}$. If in addition, the normal component of relative acceleration, a_{in}, of the contact point as it moves across the two bodies is zero (positive), then the contact is assumed to be maintained (breaking) (see [11]).

We also must precisely distinguish between sliding and rolling. Let v_{it} and v_{io} denote two orthogonal components of relative velocity in the contact tangent plane at contact i, and v_{ir} denote the relative angular velocity about the normal of contact i. If any one of these three relative velocity directions is non-zero, then the direction of the generalized contact force is completely specified (see equation (2)). If all three relative velocity components are zero, then the components of the generalized friction force are unspecified by the current state, and so must be revealed by the solution of the model, specifically by the relative contact acceleration (again, see equation (2)). Therefore, it is convenient to define the index sets $\mathcal{R}$ and $\mathcal{N}$, respectively, as the sets of rolling and non-rolling contacts; these two index sets partition $\{1, \ldots, n_c\}$. The intuition behind the selective use of velocities and accelerations in the formulation of the friction law is as follows. In the case of a non-rolling contact, the friction direction is already known, so the only unknowns are the normal components of contact force and relative acceleration. If contact is maintained at the end of the current time step (indicated by $a_{in} = 0$), then non-rolling with constant relative velocity was implicitly assumed. In the case of a rolling contact, the only way to indicate changes from rolling to non-rolling is through non-zero values of the relative accelerations components, which imply yield non-zero relative velocities that determine the direction of the generalized friction force.

Before introducing the complete model below, we must first introduce several quantities. The contact velocity components expressed in the contact frames will be denoted by $\boldsymbol{\nu} = (\boldsymbol{\nu}_n, \boldsymbol{\nu}_t, \boldsymbol{\nu}_o, \boldsymbol{\nu}_r)$, where each subvector is defined as $\boldsymbol{\nu}_\alpha = (v_{1\alpha}, v_{2\alpha}, \ldots, v_{n_c\alpha})$ for $\alpha = \{n, t, o, r\}$. For example, $\boldsymbol{\nu}_n$ is the vector of normal components of the relative velocities at the contacts. Further, denote the positive definite system inertia matrix and system constraint Jacobian as $\mathcal{M}$ and $\mathcal{J}$, respectively. The inertia matrix relates forces and moments to body accelerations, while the Jacobian relates the body velocities to the relative contact velocities. The unknowns of the model will be the vectors of relative accelerations and

contact forces and moments. Following the convention used to define $\boldsymbol{\nu}$, these are denoted by $(\boldsymbol{a}_n, \boldsymbol{a}_t, \boldsymbol{a}_o, \boldsymbol{a}_r)$ and $(\boldsymbol{c}_n, \boldsymbol{c}_t, \boldsymbol{c}_o, \boldsymbol{c}_r)$, respectively. The subscripts t and o refer to the two tangential components of the relative linear accelerations or forces at the contacts, while the subscript r refers to the relative angular acceleration or contact moment in the direction of the contact normal.

The equations and inequalities mentioned above that constitute the model are naturally partitioned into four sets as follows:

(i) the combined kinematic/Newton-Euler equations of motion,

$$\begin{bmatrix} \boldsymbol{a}_n \\ \boldsymbol{a}_t \\ \boldsymbol{a}_o \\ \boldsymbol{a}_r \end{bmatrix} = \boldsymbol{A} \begin{bmatrix} \boldsymbol{c}_n \\ \boldsymbol{c}_t \\ \boldsymbol{c}_o \\ \boldsymbol{c}_r \end{bmatrix} + \begin{bmatrix} \boldsymbol{b}_n \\ \boldsymbol{b}_t \\ \boldsymbol{b}_o \\ \boldsymbol{b}_r \end{bmatrix},$$

where $\boldsymbol{A} = \mathcal{J}^T \mathcal{M} \mathcal{J}$ is a positive semidefinite matrix of size $4n_c$, and $(\boldsymbol{b}_n, \boldsymbol{b}_t, \boldsymbol{b}_o, \boldsymbol{b}_r) = \dot{\mathcal{J}}^T \boldsymbol{\nu} + \mathcal{J}^T \mathcal{M}^{-1} \boldsymbol{g}_{\text{obj}}$ is a vector containing the known external forces applied to the system and velocity product forces; (since $\mathcal{M}$ is positive definite, the null space of $\boldsymbol{A}$ coincides with the null space of $\mathcal{J}$; in particular, $\boldsymbol{A}$ is positive definite if and only if $\mathcal{J}$ has linearly independent columns[2])

(ii) the nontensile restrictions on the contact forces, the unilateral kinematic constraints, and the complementarity conditions on the normal contact forces and accelerations,

$$0 \leq \boldsymbol{a}_n \perp \boldsymbol{c}_n \geq 0,$$

where the $\perp$ notation denotes the perpendicular relation between two vectors;

(iii) the elliptic dry friction condition suggested by Howe and Cutkosky [6] (based upon a series of contact friction experiments),

$$\frac{c_{it}^2}{e_{it}^2} + \frac{c_{io}^2}{e_{io}^2} + \frac{c_{ir}^2}{e_{ir}^2} \leq \mu_i^2 c_{in}^2, \quad i = 1, \ldots, n_c, \tag{1}$$

where e_{it}, e_{io}, and e_{ir} are given positive constants and μ_i is the coefficient of friction (assumed positive); and

(iv) the maximum work principle: for each $i \in \mathcal{N}$,

$$(c_{it}, c_{io}, c_{ir}) \in \operatorname{argmax} \left\{ \begin{array}{l} -(v_{it} c'_{it} + v_{io} c'_{io} + v_{ir} c'_{ir}) : \\ \left(\frac{c'_{it}}{e_{it}}\right)^2 + \left(\frac{c'_{io}}{e_{io}}\right)^2 + \left(\frac{c'_{ir}}{e_{ir}}\right)^2 \leq \mu_i^2 c_{in}^2 \end{array} \right\},$$

[2]Note that the restriction of linearly independent columns of $\mathcal{J}$ is very stringent, since any pair of bodies with two or more contacts will violate this condition.

and for each $i \in \mathcal{R}$,

$$(c_{it}, c_{io}, c_{ir}) \in \operatorname{argmax} \left\{ \begin{array}{l} -(a_{it}c'_{it} + a_{io}c'_{io} + a_{ir}c'_{ir}) : \\ \left(\frac{c'_{it}}{e_{it}}\right)^2 + \left(\frac{c'_{io}}{e_{io}}\right)^2 + \left(\frac{c'_{ir}}{e_{ir}}\right)^2 \leq \mu_i^2 c_{in}^2 \end{array} \right\},$$

where argmax $\{f(x) : x \in X\}$ denotes the set of optimal solutions of the maximization problem:

$$\begin{array}{ll} \text{maximize} & f(x) \\ \text{subject to} & x \in X. \end{array}$$

By formulating the above maximization problem with Lagrange multipliers as an unconstrained problem and deriving the Fritz-John optimality conditions, the maximum work principle (conditions (iv) above), can be replaced by the following equivalent system of equations:

$$\left. \begin{array}{l} e_{it}^2 \mu_i c_{in} \sigma_{it} + \sqrt{e_{it}^2\sigma_{it}^2 + e_{io}^2\sigma_{io}^2 + e_{ir}^2\sigma_{ir}^2}\, c_{it} = 0 \\ e_{io}^2 \mu_i c_{in} \sigma_{io} + \sqrt{e_{it}^2\sigma_{it}^2 + e_{io}^2\sigma_{io}^2 + e_{ir}^2\sigma_{ir}^2}\, c_{io} = 0 \\ e_{ir}^2 \mu_i c_{in} \sigma_{ir} + \sqrt{e_{it}^2\sigma_{it}^2 + e_{io}^2\sigma_{io}^2 + e_{ir}^2\sigma_{ir}^2}\, c_{ir} = 0 \end{array} \right\} \quad \forall i = 1, \ldots, n_c; \tag{2}$$

where

$$(\sigma_{it}, \sigma_{io}, \sigma_{ir}) = \left\{ \begin{array}{ll} (v_{it}, v_{io}, v_{ir}) & \text{if } i \in \mathcal{N}, \\ (a_{it}, a_{io}, a_{ir}) & \text{if } i \in \mathcal{R}. \end{array} \right.$$

In order to handle other kinds of dry friction laws, we introduce a generalized model in which we replace the quadratic friction cone defined by (1) by an abstract closed convex cone and modify the maximum work inequality accordingly. Specifically, for each $i = 1, \ldots, n_c$, let $\mathcal{F}_i : R_+ \to R^3$ be a set-valued map with the property that for each scalar $\sigma \geq 0$, the image $\mathcal{F}_i(\sigma)$ is a closed convex cone in the 3-dimensional Euclidean space R^3 and that $\mathcal{F}_i(0) = \{0\}$. The latter property of $\mathcal{F}_i$ stipulates that at each contact, if the normal force is zero, then so is the friction force and the transmitted moment.

Consider the following generalized friction conditions:

(iii)$'$ for each $i = 1, \ldots, n_c$, $(c_{it}, c_{io}, c_{ir}) \in \mathcal{F}_i(\mu_i c_{in})$;

(iv)$'$ the maximum work principle: for each $i \in \mathcal{N}$,

$$(c_{it}, c_{io}, c_{ir}) \in \operatorname{argmax}\{-(v_{it}c'_{it} + v_{io}c'_{io} + v_{ir}c'_{ir}) : (c'_{it}, c'_{io}, c'_{ir}) \in \mathcal{F}_i(\mu_i c_{in})\},$$

and for each $i \in \mathcal{R}$,

$$(c_{it}, c_{io}, c_{ir}) \in \operatorname{argmax}\{-(a_{it}c'_{it} + a_{io}c'_{io} + a_{ir}c'_{ir}) : (c'_{it}, c'_{io}, c'_{ir}) \in \mathcal{F}_i(\mu_i c_{in})\}.$$

The generalized dynamic multi-rigid-body problem with concurrent distributed frictional contacts is to find contact forces $(c_{in}, c_{it}, c_{io}, c_{ir})$ and accelerations $(a_{in}, a_{it}, a_{io}, a_{ir})$ satisfying conditions (i), (ii), (iii)$'$, and (iv)$'$.

Examples of $\mathcal{F}_i(\sigma)$ include (a) the elliptic cone (1):

$$\mathcal{F}_i(\sigma) \equiv \left\{ (c_{it}, c_{io}, c_{ir}) \in R^3 \,:\, \frac{c_{it}^2}{e_{it}^2} + \frac{c_{io}^2}{e_{io}^2} + \frac{c_{ir}^2}{e_{ir}^2} \le \sigma^2 \right\},$$

where e_{it}, e_{io}, and e_{ir} are some given positive scalars; (b) approximations of such a cone by a convex polyhedron:

$$\mathcal{F}_i(\sigma) \equiv \left\{ (c_{it}, c_{io}, c_{ir}) \in R^3 : \alpha_{ij} c_{it} + \beta_{ij} c_{io} + \gamma_{ij} c_{ir} \le \sigma,\, j = 1, \ldots, m_i \right\},$$

where α_{ij}, β_{ij} and γ_{ij} are some given scalars and m_i is a positive integer; and (c) mixtures of elliptic and polyhedral friction constraints: *e.g.*,

$$\mathcal{F}_i(\sigma) \equiv \left\{ (c_{it}, c_{io}, c_{ir}) \in R^3 \,:\, \frac{c_{it}^2}{e_{it}^2} + \frac{c_{io}^2}{e_{io}^2} \le \sigma^2, |c_{ir}| \le \sigma \right\}.$$

For planar problems, we can let

$$\mathcal{F}_i(\sigma) \,\equiv\, \{(c_{it}, 0, 0) \in R^3 \,:\, |c_{it}| \le \sigma\}.$$

Examples (a) and (c) pertain to axi-symmetric friction laws; whereas (b) do not necessary correspond to such laws. Other axi-asymmetric friction laws can also be modeled by using the friction map $\mathcal{F}_i$.

3 Existence and Uniqueness of Solutions

Employing a unified approach, we provide sufficient conditions for the existence and uniqueness of solutions to the basic model presented in the last section. Similar results can be established for variations of this model, such as those based on the abstract friction maps $\mathcal{F}_i$. Due to space limitations, we will focus our discussion on the basic model under the quadratic dry friction law with torsional friction.

Let $\mathcal{F}$ consist of all force tuples (c_n, c_t, c_o, c_r) such that $c_n \ge 0$,

$$\left.\begin{aligned} e_{it}^2 \mu_i c_{in} v_{it} + \sqrt{e_{it}^2 v_{it}^2 + e_{io}^2 v_{io}^2 + e_{ir}^2 v_{ir}^2}\, c_{it} = 0 \\ e_{io}^2 \mu_i c_{in} v_{io} + \sqrt{e_{it}^2 v_{it}^2 + e_{io}^2 v_{io}^2 + e_{ir}^2 v_{ir}^2}\, c_{io} = 0 \\ e_{ir}^2 \mu_i c_{in} v_{ir} + \sqrt{e_{it}^2 v_{it}^2 + e_{io}^2 v_{io}^2 + e_{ir}^2 v_{ir}^2}\, c_{ir} = 0 \end{aligned}\right\} \forall i \in \mathcal{N},$$

and

$$\frac{c_{it}^2}{e_{it}^2} + \frac{c_{io}^2}{e_{io}^2} + \frac{c_{ir}^2}{e_{ir}^2} \le \mu_i^2 c_{in}^2, \quad \forall i \in \mathcal{R}.$$

Let

$$\mathcal{F}_{\mathcal{J}} \equiv \mathcal{F} \cap \text{ null space of } \mathcal{J}.$$

The main result of this paper is summarized in the following theorem.

Theorem 1 *Let $\boldsymbol{A} \equiv \mathcal{J}^T \mathcal{M} \mathcal{J}$ with $\mathcal{M}$ being symmetric positive definite.*

(A) If $\boldsymbol{A}$ is positive definite, then there exists a scalar friction bound $\bar{\mu} > 0$ such that whenever $\mu_i \in [0, \bar{\mu}]$ for all $i \in \mathcal{N}$, there exist

$$(\boldsymbol{a}_n, \boldsymbol{a}_t, \boldsymbol{a}_o, \boldsymbol{a}_r) \quad \textit{and} \quad (\boldsymbol{c}_n, \boldsymbol{c}_t, \boldsymbol{c}_o, \boldsymbol{c}_r)$$

solving the rigid-body contact model defined by conditions (i)–(iv). If in addition $\mu_i \in [0, \bar{\mu}]$ for all $i \in \mathcal{R}$, then the solution is unique.

(B) If $\mathcal{N} = \emptyset$, and

$$\begin{bmatrix} \boldsymbol{b}_n \\ \boldsymbol{b}_t \\ \boldsymbol{b}_o \\ \boldsymbol{b}_r \end{bmatrix}^T \begin{bmatrix} \boldsymbol{c}_n \\ \boldsymbol{c}_t \\ \boldsymbol{c}_o \\ \boldsymbol{c}_r \end{bmatrix} \geq 0 \quad \textit{for all} \quad \begin{bmatrix} \boldsymbol{c}_n \\ \boldsymbol{c}_t \\ \boldsymbol{c}_o \\ \boldsymbol{c}_r \end{bmatrix} \in \mathcal{F}_{\mathcal{J}},$$

then for any positive $\{\mu_i : i = 1, \ldots, n_c\}$, the first conclusion of (A) holds.

The conditions in the two statements (A) and (B) of the theorem are different. The conditions in (A) require the entire matrix $\boldsymbol{A}$ be positive definite and the friction coefficients at the non-rolling contacts be small; in this case if the friction coefficients at the rolling contacts are also sufficiently small, then the solution must be unique. A theoretical estimate for the friction bound $\bar{\mu}$ can be computed as discussed in [15]. Such an estimate tends to be very conservative and can be expected to be much smaller than one would expect to encounter in real systems.

Part (B) pertains to the all-rolling case. In this case, there is no condition imposed on the friction coefficients; also $\boldsymbol{A}$ is not required to be positive definite. The proofs of Theorem 1 are straight forward extensions of those in the papers [10, 15]; background results needed in the proofs are in [2, 4].

4 Example Problems

Two simple multi-rigid-body systems were simulated using two different time-stepping methods; a first-order, explicit method (referred to as the Stewart method [13]) based on forward Euler time-stepping and a linearized dynamic model, and a first-order, implicit method (referred to as the Tzitzouris-Pang method [17, 18]) based on backward Euler time-stepping and the full nonlinear dynamic model. While both of these methods have been reformulated around more accurate time-stepping schemes, the comparison presented here is limited to the Euler methods.

To apply the Stewart method one approximates each friction cone as a convex polyhedron in the space of generalized friction force directions and each active nonpenetration constraint,

$\psi_{in} \geq 0$, as a linear inequality. After replacing the acceleration and velocity variables with their forward differences divided by the integration time interval, h, one formulates a linear complementarity problem (LCP). The solution of this LCP is the contact impulses that guarantee the consistency of the linearized model and maximum work inequality at the end of the current time interval. The impulses obtained are then used to compute the corresponding new body velocities and positions, without ever computing the accelerations. To advance the state another time step, the system is linearized about its new configuration and another LCP is formulated and solved.[3]

The Tzitzouris-Pang method (see [18]) retains the nonlinear features of the dynamic model and therefore leads to a (mixed) nonlinear complementarity problem (NCP) to be solved at each time step. An implicit time-stepping method was employed in the Tzitzouris-Pang method, because it was expected that the bulk of the computational work for each time step would be devoted to the solution of the NCP rather than the implicit equations.[4] Similar to the Stewart method, the subproblems solved in the Tzitzouris-Pang method guarantee consistency with the (nonlinear) model at the end of the current time interval. One difference between the methods is that the Tzitzouris-Pang subproblems are written in terms of acceleration and force variables, which are obtained by solving the mixed NCP and are then integrated numerically to obtain the configuration and velocity variables. The NCPs were solved by a "hot-starting" Bouligand differentiable (B-diff) Newton algorithm [3, 9]. For sufficiently small step sizes, using the previous solution as a starting point for the new NCP was quite effective.

Since the methods were implemented on different platforms and languages (Matlab and C++) and require the solution of quite different numerical problems at each step, our comparison is limited to accuracy. While direct cpu time comparisons would not be meaningful, our experience indicates that the Tzitzouris-Pang method is likely to be faster and more accurate than the Stewart, but more difficult to implement.

4.1 System 1: Sphere on Plane

Figure 2 shows an elevation view of a uniform sphere in contact with a fixed half-space in a uniform gravitational field. This example was chosen, because the "surface" constraint in configuration space is planar. As such, it removed one of the sources of difference between the Stewart and Tzitzouris-Pang methods. The primary difference between the two methods for this problem then was the linearization of the friction law.

For the sphere/plane problem, the surface of the fixed half-space coincides with the xy-plane of the (right-handed) inertial frame, with the inertial z-direction parallel to the outward normal of the half-space. The normal axis, $\hat{\boldsymbol{n}}$, of the contact frame always points in the inertial z-direction. The $\hat{\boldsymbol{t}}$ and $\hat{\boldsymbol{o}}$ directions lie in the inertial xy-plane rotated $\frac{\pi}{4}(R)$ from

[3]The LCPs of the Stewart method were solved using Lemke's algorithm provided by Michael Ferris, University of Wisconsin at Madison.

[4]This expectation was born out in our experiments.

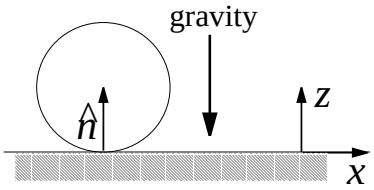

Figure 2: Sphere on a Half-Space.

the inertial x and y axes. In addition, the mass matrix, $\mathcal{M}$, the Jacobian matrix, $\mathcal{J}$, the external generalized force, $\boldsymbol{g}_{\text{obj}}$, and the position of the contact with respect to the center of the sphere (expressed in the inertial frame), are all constant. Given this information and assuming the sphere has unit mass and radius the Jacobian and mass matrices and generalized external force can be shown to be:

$$\mathcal{M} = \begin{bmatrix} \boldsymbol{E}_3 & 0 \\ 0 & \frac{2}{5}\boldsymbol{E}_3 \end{bmatrix}, \qquad \mathcal{J} = \begin{bmatrix} 0 & \frac{\sqrt{2}}{2} & -\frac{\sqrt{2}}{2} & 0 \\ 0 & \frac{\sqrt{2}}{2} & \frac{\sqrt{2}}{2} & 0 \\ 1 & 0 & 0 & 0 \\ 0 & \frac{\sqrt{2}}{2} & \frac{\sqrt{2}}{2} & 0 \\ 0 & -\frac{\sqrt{2}}{2} & \frac{\sqrt{2}}{2} & 0 \\ 0 & 0 & 0 & 1 \end{bmatrix}, \qquad \boldsymbol{g}_{\text{obj}} = \begin{bmatrix} 0 \\ 0 \\ -9.81 \\ 0 \\ 0 \\ 0 \end{bmatrix}.$$

Substituting these quantities into the definitions of $\boldsymbol{A}$ and $\boldsymbol{b}$ defined in section 2 yields:

$$\boldsymbol{A} = \mathcal{J}^T\mathcal{M}^{-1}\mathcal{J} = \begin{bmatrix} 1 & 0 & 0 & 0 \\ 0 & 3.5 & 0 & 0 \\ 0 & 0 & 3.5 & 0 \\ 0 & 0 & 0 & 2.5 \end{bmatrix}, \qquad \boldsymbol{b} = \dot{\mathcal{J}}^T\boldsymbol{\nu} + \mathcal{J}^T\mathcal{M}^{-1}\boldsymbol{g}_{\text{obj}} = \begin{bmatrix} 9.81 \\ 0 \\ 0 \\ 0 \end{bmatrix}. \tag{3}$$

4.1.1 Problem 1, Experiment 1: Sphere Rotating in Place

In this problem, the sphere was placed on the plane and released with angular velocity normal to the plane with all other velocity components zero.[5] The specific data for this problem was:

$$\left.\begin{array}{ll} \text{initial configuration:} & \boldsymbol{q} = [0\ 0\ 1 \mid 1\ 0\ 0\ 0]^T \\ \text{initial velocity:} & \boldsymbol{\nu} = [0\ 0\ 0 \mid 0\ 0\ 1.962]^T \\ \text{friction parameters:} & e_t = e_o = 1 \quad e_r = 0.4 \quad \mu = 0.2. \end{array}\right\} \tag{4}$$

where the first three components of the initial configuration represent the position of the center of the sphere and the last four components are the Euler parameters (or unit quaternion) defining the orientation of the sphere's body-fixed frame (origin at the center of the

[5]Other experiments in which the sphere initially translated can be found in [16].

sphere) relative to the inertial frame. The values [1 0 0 0] indicate that the body axes were initially aligned with those of the inertial frame. The first and last three components of the generalized velocity, $\boldsymbol{\nu}$, are the linear and angular velocities, respectively, of the sphere with respect to the inertial frame.

Figure 3 shows the nonlinear surface of the friction ellipsoid in the space of friction directions, c_t, c_o, and c_r, used by the Tzitzouris-Pang method. It also shows the directions (indicated by the small spheres embedded in the ellipsoid) used to linearize the ellipsoid for the Stewart method. The columns in Equation (5) correspond to these directions.

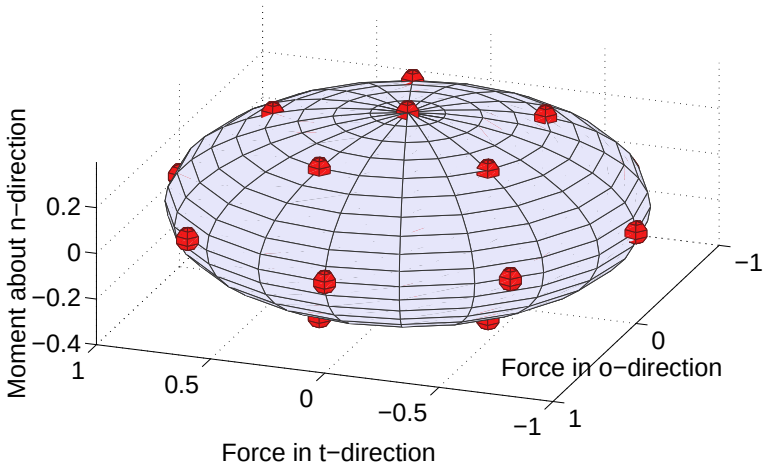

Figure 3: Friction Ellipsoid (equation (1)) for Problem 1, Experiment 1 with $c_n = 5$.

$$
D = \begin{bmatrix}
0.7071 & 0.0000 & -0.7071 & -1.0000 & -0.7071 & -0.0000 & 0.7071 & 1.0000 & 0.4177 & -0.2682 \\
0.7071 & 1.0000 & 0.7071 & 0.0000 & -0.7071 & -1.0000 & -0.7071 & -0.0000 & 0.4177 & 0.5264 \\
0 & 0 & 0 & 0 & 0 & 0 & 0 & 0 & 0 & 0 \\
0.7071 & 1.0000 & 0.7071 & 0.0000 & -0.7071 & -1.0000 & -0.7071 & -0.0000 & 0.4177 & 0.5264 \\
-0.7071 & -0.0000 & 0.7071 & 1.0000 & 0.7071 & 0.0000 & -0.7071 & -1.0000 & -0.4177 & 0.2682 \\
0 & 0 & 0 & 0 & 0 & 0 & 0 & 0 & 0.3227 & 0.3227
\end{bmatrix} \cdots
$$

$$
\cdots \begin{bmatrix}
-0.5835 & -0.0924 & 0.5264 & 0.4177 & -0.2682 & -0.5835 & -0.0924 & 0.5264 & 0.0000 & 0.0000 \\
-0.0924 & -0.5835 & -0.2682 & 0.4177 & 0.5264 & -0.0924 & -0.5835 & -0.2682 & 0.0000 & 0.0000 \\
0 & 0 & 0 & 0 & 0 & 0 & 0 & 0 & 0 & 0 \\
-0.0924 & -0.5835 & -0.2682 & 0.4177 & 0.5264 & -0.0924 & -0.5835 & -0.2682 & 0.0000 & 0.0000 \\
0.5835 & 0.0924 & -0.5264 & -0.4177 & 0.2682 & 0.5835 & 0.0924 & -0.5264 & -0.0000 & -0.0000 \\
0.3227 & 0.3227 & 0.3227 & -0.3227 & -0.3227 & -0.3227 & -0.3227 & -0.3227 & 0.4000 & -0.4000
\end{bmatrix}. \quad (5)
$$

Using a time step of 0.07 seconds, the dynamics were integrated for approximately 1.2 seconds of simulated time using the Stewart and Tzitzouris-Pang methods. Both methods returned identical results. From the symmetry of the problem, one can see that the sphere should rotate in place with constant deceleration to zero. Therefore, the plot of $v_r(t) = \omega_z(t)$ should decrease linearly from its initial value to zero. Figure 4 shows the analytical solution for the ω_z as a fine dotted line of slope equal to -1.962(Rad/s^2). The circles on that line are the velocity components predicted by the time-stepping methods, while the light circles on the horizontal axis are the values of the other 5 velocity components (all zero) of the sphere.

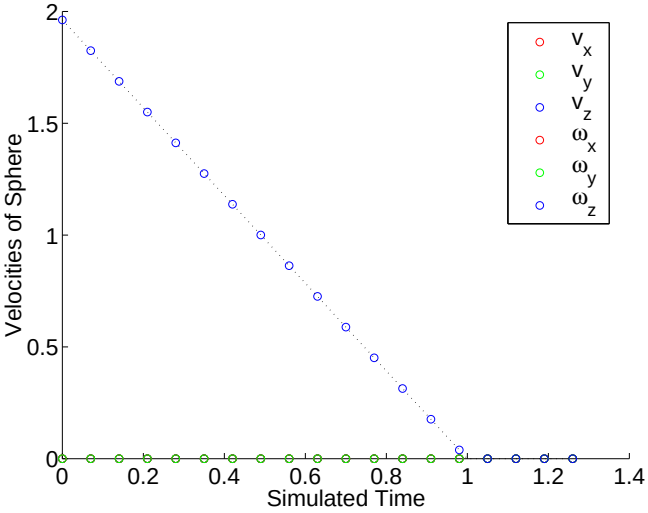

Figure 4: Numerical vs. Analytical Velocities for Problem 1, Experiment 1.

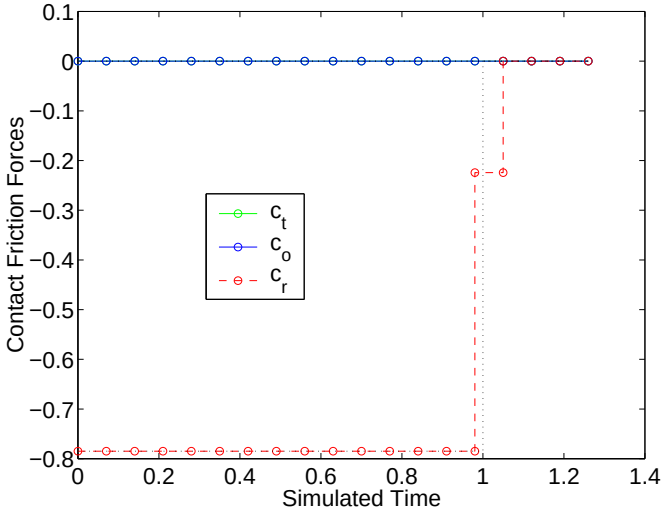

Figure 5: Numerical vs. Analytical Forces for Problem 1, Experiment 1.

Since the form of $\omega_z(t)$ implied by the time-stepping methods are piecewise linear between the solution points, only in the time step from $t = 0.98$ to $t = 1.05$ did the analytical and numerical solutions disagree. This mismatch was due to the fact that the time at which spinning stopped did not appear in the sequence of times used for integration. It should also be noted that the Stewart method matched the exact solution, only because one of the friction directions (column 20, in equation (5)) corresponded to the exact solution, thereby eliminating the friction linearization error.

Consistent with the velocity plot, the friction force plot in Figure 5 shows good agreement between the numerical and exact solutions. While not shown, the normal component of the contact force, c_n, was equal to mg for all time. The tangential components of the contact force, c_t and c_o, plotted as circles connected by solid line segments, were zero as expected. The torsional component of the contact force, c_r, plotted as a circles connected by dashed line segments, shows the prediction error clearly in the time step containing $t = 1.0$. However, despite this error, the total frictional impulse was correct since the sphere stopped spinning. Again, the Tzitzouris-Pang and Stewart methods produced identical force values at the times of evaluation.

Since the direction of the friction moment was known *a priori* to be constant and in the $-z$-direction for all time in this problem, it was possible to rerun the problem with only that friction direction in the matrix $\boldsymbol{D}$, so that all LCPs solved in the Stewart method were of size 3 rather than 22. However, when the initial conditions were changed to include translational velocity components parallel to the plane, the sphere translated indefinitely (due to the lack of a friction force to resist translational slipping). While such an example is physically unreasonable, it demonstrated that friction linearization and the Stewart method can be

easily used to model the behavior of systems with unusual anisotropic friction behavior.

4.1.2 Problem 1, Experiment 2: Sphere Rotating in Place

The Stewart method was applied to the same problem again, but with the set of friction direction vectors shown in Figure 6; none of which pointed in the direction of the exact generalized frictional force. The misalignment of the friction directions effectively reduced the frictional moment and led to slower deceleration of the spinning sphere (see Figures 7 and Figures 8; the dotted black line represents the exact solution.) Notice that while the friction work rate was reduced, the total torsional impulse delivered to the sphere was identical to that predicted analytically. However, the impulses delivered in the t and o directions was not quite zero, leading to a very small residual velocity after spinning stopped.

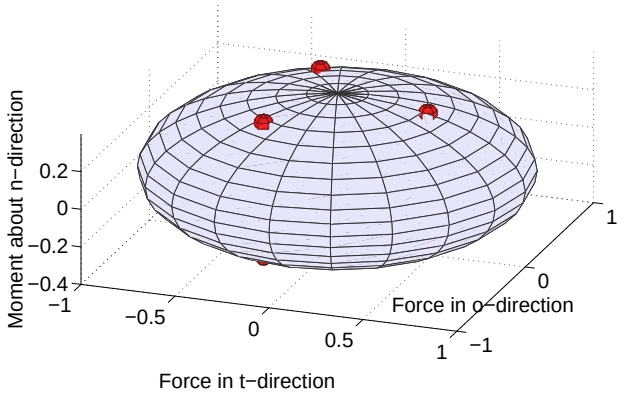

Figure 6: Friction Ellipsoid for Problem 1, Experiment 2 with $c_n = 5$.

$$D = \begin{bmatrix} 0.3410 & -0.4659 & 0.1248 & 0.3410 & -0.4659 & 0.1248 \\ 0.3410 & 0.1248 & -0.4659 & 0.3410 & 0.1248 & -0.4659 \\ 0 & 0 & 0 & 0 & 0 & 0 \\ 0.3410 & 0.1248 & -0.4659 & 0.3410 & 0.1248 & -0.4659 \\ -0.3410 & 0.4659 & -0.1248 & -0.3410 & 0.4659 & -0.1248 \\ 0.3504 & 0.3504 & 0.3504 & -0.3504 & -0.3504 & -0.3504 \end{bmatrix}. \tag{6}$$

4.1.3 Problem 2, Experiment 1: Initially Translating Sphere

In this experiment, the sphere was released in contact with the plane with zero angular velocity. Only the x-component of linear velocity was nonzero. The initial conditions and friction model parameters that defined this example were:

$$\begin{aligned} &\text{initial configuration:} && \boldsymbol{q} = [0\ 0\ 1 \mid 1\ 0\ 0\ 0]^T \\ &\text{initial velocity:} && \boldsymbol{\nu} = [2\ 0\ 0 \mid 0\ 0\ 0]^T \\ &\text{friction parameters:} && e_t = e_o = 1 \quad e_r = 0.4 \quad \mu = 0.2, \end{aligned} \tag{7}$$

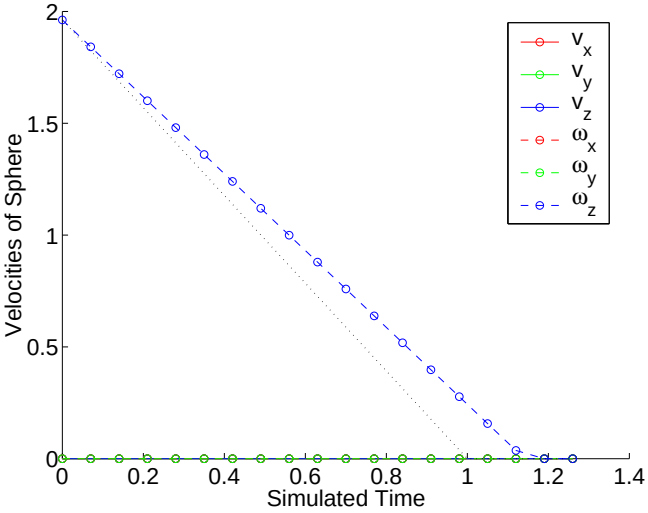

Figure 7: Numerical vs. Analytical Velocities for Problem 1, Experiment 2.

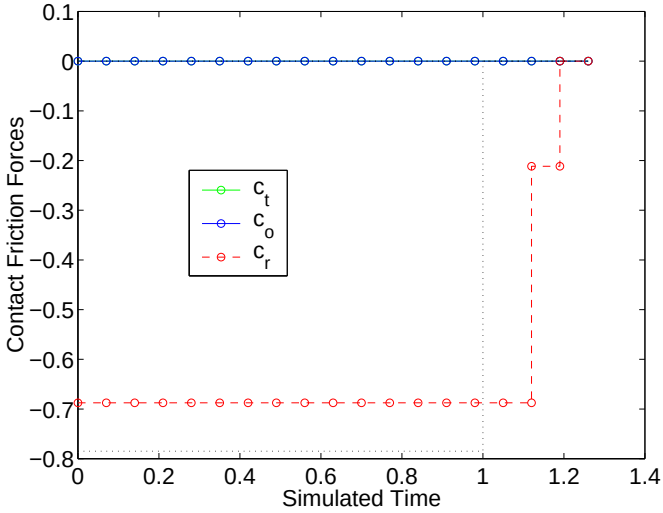

Figure 8: Numerical vs. Analytical Forces for Problem 1, Experiment 2.

The friction model and linearization used in this example were the same as those used in the first problem (see Figure 3).

For problem 2, experiment 1, the exact solution of the sphere's motion was obtained analytically. It was found that the sphere would initially slide in the x-direction, gathering angular velocity in the y-direction until the transition time, $t_{trn} = \frac{2v_{x_0}}{7\mu g} \approx 0.291$, where v_{x_0} is the initial velocity in the x-direction. After the transition time, the sphere would roll with constant velocity along the x-axis and angular velocity $\omega_y = \frac{5}{7}v_{x_0} \approx 1.429$. The remaining 4 velocity components would be zero (i.e., $v_y = v_z = \omega_x = \omega_z = 0$).

The numerical solution for this experiment was computed over the time interval [0, 0.6]. Both methods matched the exact velocities as shown in Figure 9, which plots the sphere's velocity components and the exact solution (as dotted lines). It should be noted that the Stewart method only matched the exact solution, because one of the friction directions (column 7, in equation (5)) was pointing exactly in the $-x$-direction. Since every nonzero friction force for this problem was acting in this direction, the friction cone linearization error was zero. Since the Tzitzouris-Pang method uses the nonlinear friction cone, it cannot suffer from a similar problem.

Figure 10 shows the components of the friction force over time as predicted by the two methods, which both implicitly assume piecewise constant forces. Thus, the stair-step look of the plots in the figure. Note that both c_t and c_o were nonzero due to the misalignment of the $\hat{\boldsymbol{t}}$ and $\hat{\boldsymbol{o}}$ directions with respect to the x- and y-axes. Again, the analytical solution is plotted with dotted lines.

This experiment was rerun with the same data as given in equations (7) and (5), but

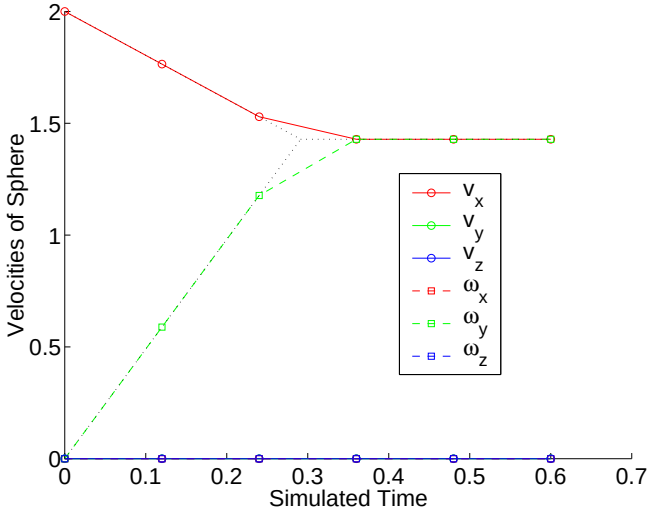

Figure 9: Numerical and Analytical Velocities: Both Time-Stepping Methods, $h = 0.12$.

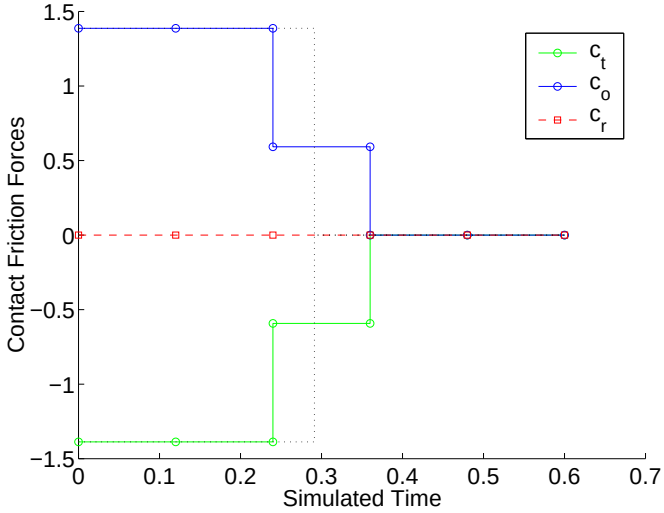

Figure 10: Numerical and Analytical Forces: Both Time-Stepping Methods, $h = 0.12$.

with the step size reduced by a factor of 10. The results demonstrated convergence to the exact solution with decreasing step size.

4.1.4 Problem 2, Experiment 2: Initially Translating Sphere

A second numerical experiment was run with the Stewart method with the same initial conditions (7), but with friction directions chosen such that no vector was aligned with the $-x$-direction (see Figure 11): Further, in the crucial tangent plane of the contact force, only three friction directions were used. Figures 12 and 13 show reduced frictional impulses

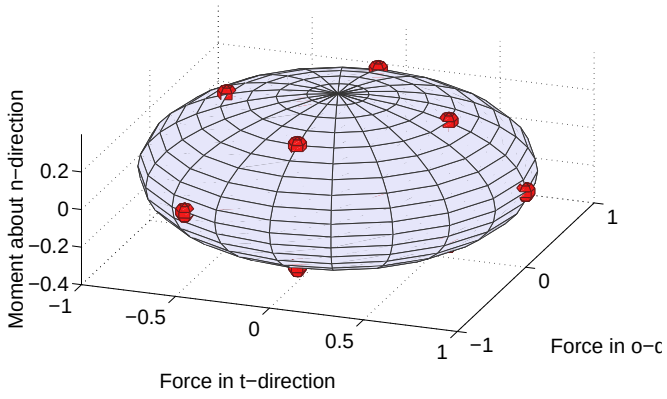

Figure 11: Friction Ellipsoid for Problem 2, Experiment 1 with $c_n = 5$.

and a longer sliding period. This was caused by the misalignment of the friction directions available in the linearized friction model. However, since the Stewart method is based on the first integral of Newton's second law, the total impulse applied at the contact matches that of the exact solution. Hence, the final rolling velocity of the sphere agrees with the analytical result.

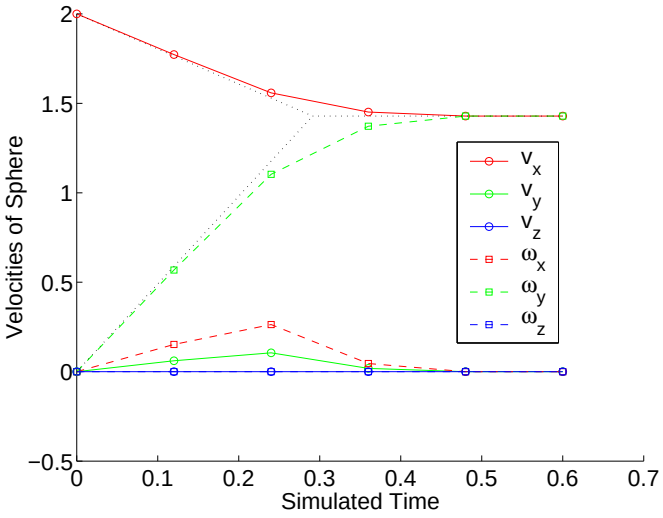

Figure 12: Numerical and Analytical Velocities for Problem 2, Experiment 2: Stewart method, $h = 0.12$.

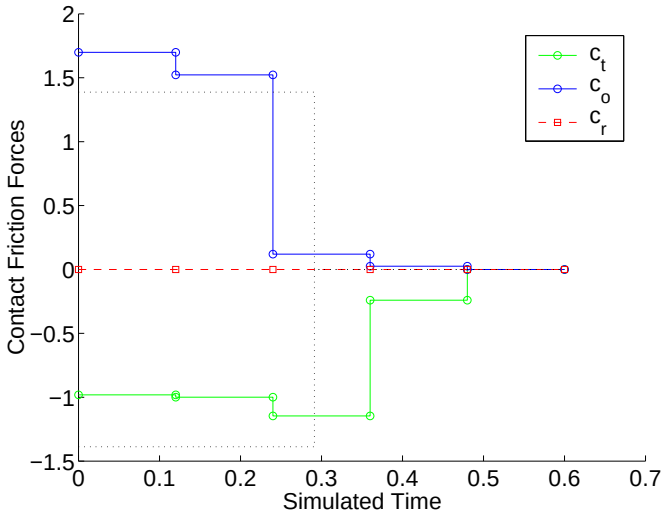

Figure 13: Numerical and Analytical Forces for Problem 2, Experiment 2: Stewart method, $h = 0.12$.

4.1.5 Problem 3: Hooking Bowling Ball

The third problem was designed to simulate a hooking bowling ball. The ball was released in contact with the plane with linear velocity in the direction of the lane's axis (the x-axis). Its initial angular velocity components were intended to cause the ball to curve as it moved down the lane (generally in the x-direction). Since oil is usually present on bowling lanes (to reduce friction and make the behavior of balls more uniform over a variety of lanes), the effective coefficient of friction was chosen to be very small; $\mu = 0.01$. The viscous friction generated by the oil was not modeled, but could be included in $\boldsymbol{g}_{\text{obj}}$ if desired. The initial conditions and friction parameters defining this problem were:

$$\begin{array}{ll} \text{initial configuration:} & \boldsymbol{q} = [0 \;\; 0.5 \;\; 1.0 \;\; | \;\; 1 \;\; 0 \;\; 0 \;\; 0]^T \\ \text{initial velocity:} & \boldsymbol{\nu} = [1 \;\; 0.2 \;\; 0 \;\; | \;\; 1 \;\; 0.5 \;\; 0.2]^T \\ \text{friction parameters:} & e_t = e_o = 1 \quad e_r = 0.2 \quad \mu = 0.01. \end{array} \tag{8}$$

The friction linearization for the Stewart method used 40 friction directions spaced uniformly around 7 latitude circles. Thus, the LCPs arising in the Stewart method for this problem were of size 42.

This problem was integrated by both methods for 8.0 seconds of simulated time using a step size of 0.05 seconds. Several aspects of the solution should be noted. First, the gross behavior predicted by both methods was essentially identical. As expected, the ball hooked as it moved down the lane (see Figure 16). Second, the frictional force components, while small (their magnitudes are less than 1% of the normal impulse) were saturated for most of the 8 seconds of simulated time, implying that the contact was sliding. After this time, the sphere began pure rolling. Last, the friction forces obtained with the Tzitzouris-Pang method were larger in magnitude and varied smoothly over time. These differences were due directly to linearizing the friction ellipsoid by an inscribed polyhedron. A consequence was that the Tzitzouris-Pang method predicted that sliding would stop more quickly, as shown in Figure 14. When the dashed curves reach zero near $t = 8(sec)$, sliding ceases. The curve that reaches zero first, about $0.4(sec)$ sooner is that predicted by the Tzitzouris-Pang method. While there were also differences in the final trajectory of the ball, they were too small to be seen in a plot.

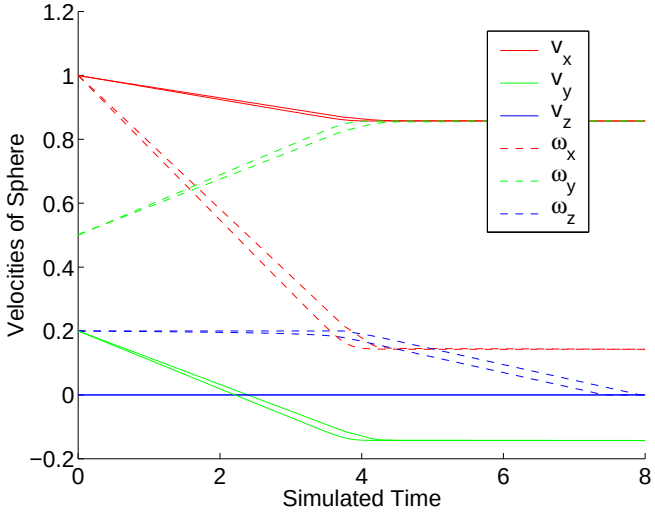

Figure 14: Velocity components: both time-stepping methods, $h = 0.05$.

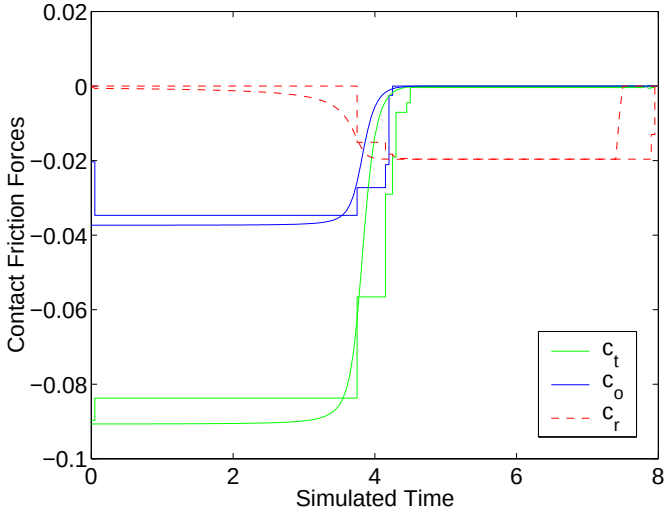

Figure 15: Friction force components, both time-stepping methods, $h = 0.05$.

Figure 17 shows the details of the friction errors during the simulation. The dashed line is a boolean variable indicating when there is relative sliding at the contact (the value 0.13 was arbitrarily chosen to imply sliding). In this problem, the contact was sliding in the interval [0, 7.9] seconds. Interestingly, the friction force components found by the Stewart method were not always saturated. If the friction components had always lain along one of the linearizing directions, then friction would have been saturated (as indicated by the zero value of the friction slack from about the 4.5 second mark). The nonzero slack during the beginning of the simulation was caused by the algorithm's finding a solution with the friction force formed by a positive linear combination of two of the initial friction directions. Such

linear combinations lie strictly inside the friction ellipsoid, and thus caused nonzero slackness in the friction ellipsoid constraint. The last feature of figure 17 worth noting, was that after sliding converted to rolling, the friction force was always zero, and hence the friction slack was maximized.

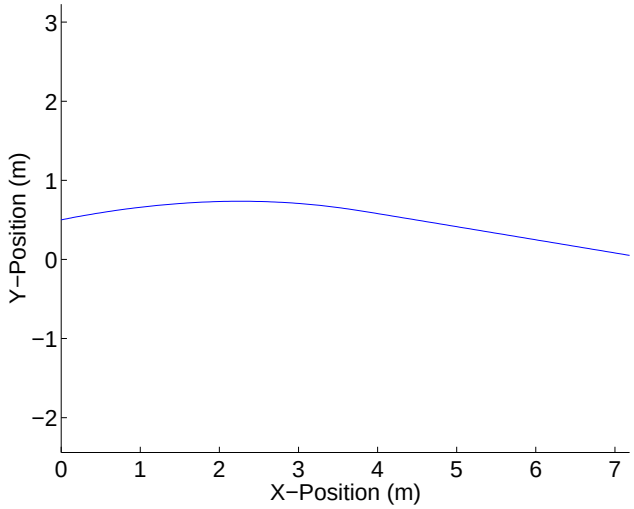

Figure 16: Path of the bowling ball as it moved down the lane toward the right: both time-stepping methods, $h = 0.05$.

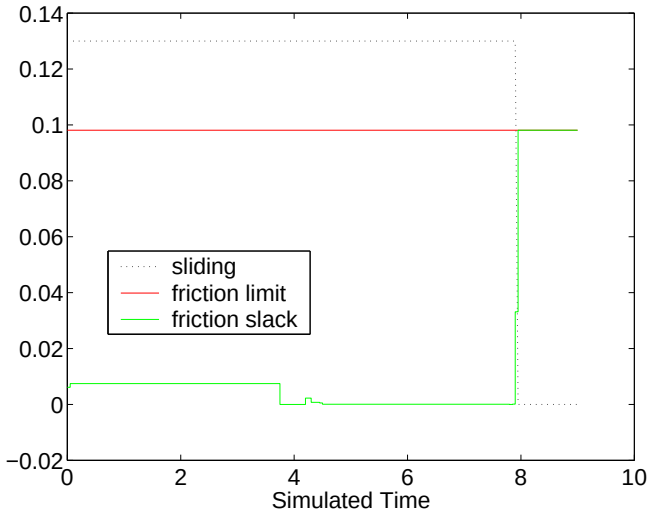

Figure 17: Friction force errors and slackness: Stewart method, $h = 0.05$.

4.2 System 2: Sphere on Spherical Surfaces

Figure 18 shows a small sphere of unit radius in simultaneous contact with two large, fixed spheres. The sphere of radius 10 is centered at the origin of the inertial frame, while the origin of the sphere of radius 9 is located at the point, (0, 11.4, 0). The small sphere began at rest, but under the influence of an external force ($\boldsymbol{g}_{\text{obj}} = [1.0 \;\; 2.6 \;\; -9.81 \;\; 0 \;\; 0 \;\; 0]^T$) that drove it rolling and sliding along the seam between the two fixed spheres. This particular example was chosen because the contact constraints in configuration space were nonlinear and because there were two simultaneous contacts. Therefore, in comparing the two time-stepping methods, we expected to see the effects of linearizing the friction model and of linearizing the distance functions $\psi_{in}, i = 1, 2$. In addition, since these contacts converted from rolling to sliding to breaking, solution by DAE methods would have been awkward.

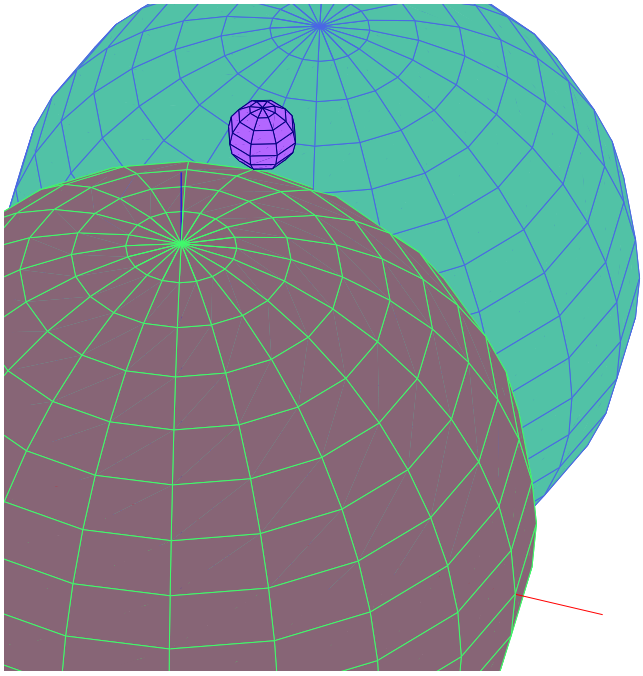

Figure 18: Small Sphere in Contact with Two Large Fixed Spheres.

The data used for this experiment were:

$$\begin{aligned}
&\text{initial configuration:} && \boldsymbol{q} = [0 \;\; 6.62105263157895 \;\; 8.78417110772903 \mid 1 \; 0 \; 0 \; 0]^T \\
&\text{initial velocity:} && \boldsymbol{\nu} = [0 \; 0 \; 0 \mid 0 \; 0 \; 0]^T \\
&\text{friction parameters:} && e_t = e_o = 1 \quad e_r = 0.3 \quad \mu = 0.2
\end{aligned} \tag{9}$$

The friction linearization for the Stewart method used the same 20 directions shown in Figure 3. Thus, the LCPs were of size 44 for two contacts or of size 22 for one.

The motion of the moving sphere was simulated by both methods using a time step of 0.1 seconds. Figures 19 and 20 show the velocities of the moving sphere and the forces

at one contact predicted by the Stewart method. Note the nonsmoothness of the velocity components that become obvious at $t \approx 2$. These discontinuities are due to the fact that even though the linear nonpenetration constraints were satisfied at the end of every time step, the nonlinear constraints were violated. As the speed of the moving sphere increased, the penetrations became larger, causing the method to predict large impulses, that ultimately caused the moving sphere to bounce back and forth across the gap until contact was lost permanently at $t \approx 3.6$ seconds.

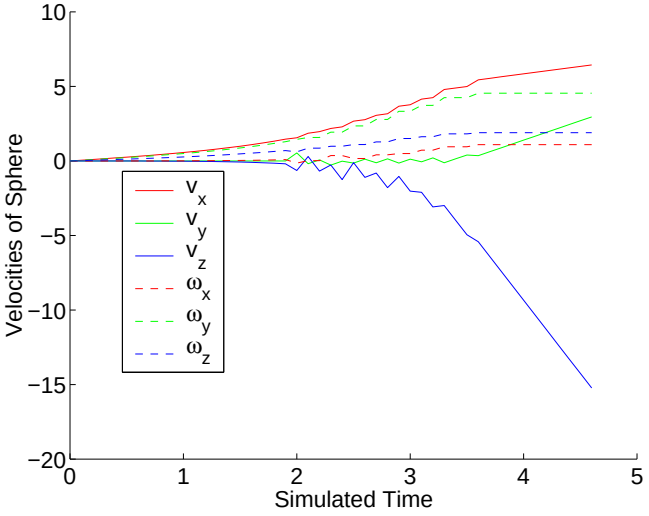

Figure 19: Velocities of the Moving Sphere: Stewart Method, $h = 0.1$.

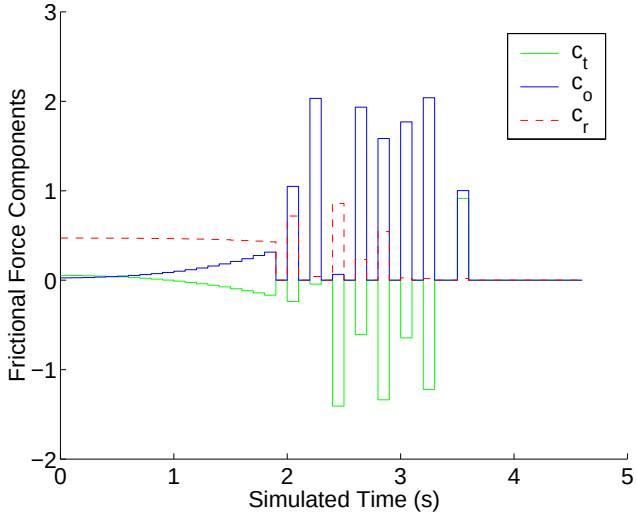

Figure 20: Forces at One Contact: Stewart Method, $h = 0.1$. The normal force component at this contact and all the force components at the other contact behaved similarly.

The Tzitzouris-Pang method, using $h = 0.1$, produced considerably smoother results (see Figures 21 and 22). This experiment was rerun using the Stewart method in an attempt to obtain comparable results. For each run, the step size was reduced by a factor of 3. At $h = 0.0012$, the unstable bouncing phenomenon disappeared and, despite the linearization, the force and state trajectories agreed well with those produced by the Tzitzouris-Pang method. However, differences in the contact forces, shown in Figure 23, caused noticeable differences in the velocities beginning at $t \approx 2(seconds)$ in Figure 24.

This experiment also highlighted somewhat unexpected behavior of the Stewart method in the force plots as the step size shrank toward zero. Figure 25 shows chattering of the torsional friction force amidst otherwise smooth behavior of the state trajectories. This was not brought about by any apparent physical phenomena. Rather, it appears to have been purely numerical and worsened as the step size was reduced beyond $h = 0.0012$.

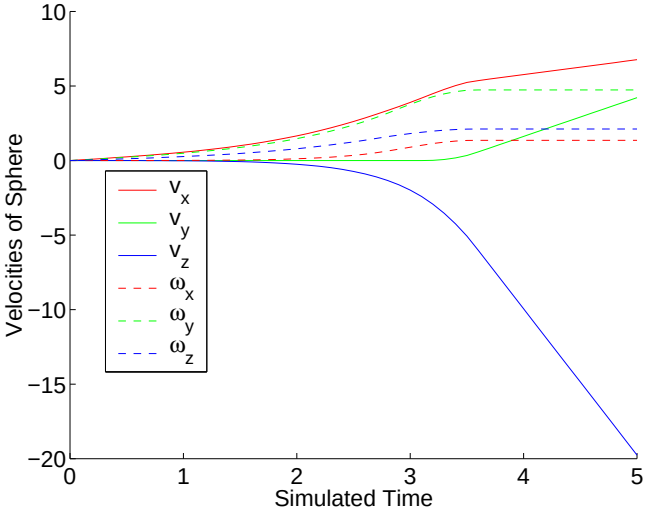

Figure 21: Velocities: Tzitzouris-Pang, $h = 0.1$.

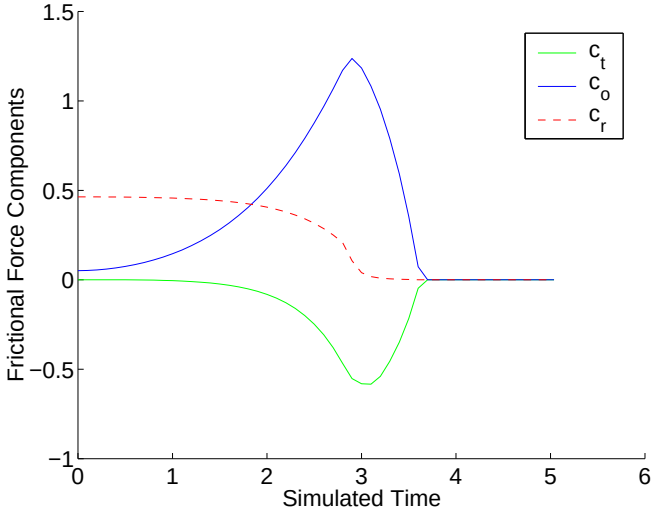

Figure 22: Forces at One Contact: Tzitzouris-Pang, $h = 0.1$.

5 Conclusion

We have formulated the dynamic equations of a general, spatial, multi-rigid-body system with multiple distributed contacts as a complementarity problem, and provided two sufficient conditions for solution existence and uniqueness. The first condition guaranteeing solution existence requires linear independence of the columns of the system Jacobian and constrains the maximum coefficient of friction at the non-rolling contacts. If the coefficients of friction at the rolling contacts are also small, then the solution is unique. The second condition guaranteeing existence pertains to problems in which all contacts are initially rolling (without twisting). It is important to note that the latter condition does *not* restrict the coefficients of friction.

We have also simulated two simple problems using an explicit method with a linearized model and an implicit method with the nonlinear model. The results have shown the practicality of the nonlinear method and highlighted the importance of retaining the nonlinear features even for very simple problems. While the Tzitzouris-pang method is more difficult to implement, it's ability to take large time-steps in problems with significant nonlinearities should not be under-appreciated.

There remain a number of open questions. On the theoretical side, we have not yet developed an efficient procedure for determining the friction bound, $\bar{\mu}$. More generally, an algorithm to determine solution uniqueness is desirable (in some situations) as a means for delineating the domain of applicability of the multi-rigid-body model. Last, there is a need to develop existence and uniqueness conditions for general situations characterized by a system Jacobian without full column rank. In the area of time-stepping methods, it would be desirable to establish similar convergence results for the Tzitzouris-Pang implicit method

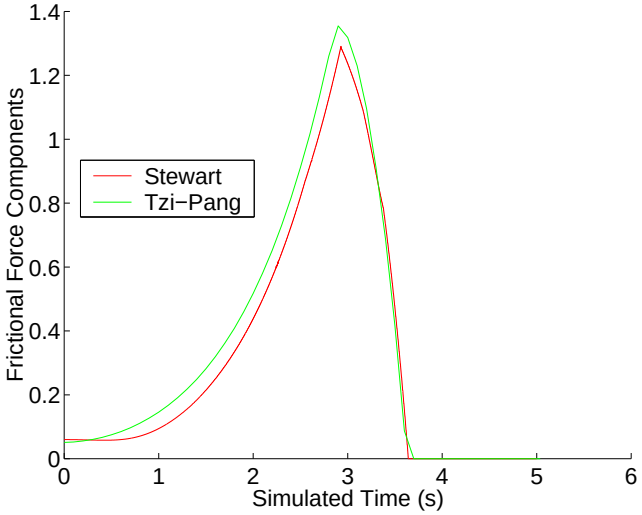

Figure 23: Magnitude of Tangential Friction Force at One Contact: Stewart, $h = 0.0012$ and Tzitzouris-Pang, $h = 0.1$. The cusps in the plots coincide with a conversion from rolling to sliding.

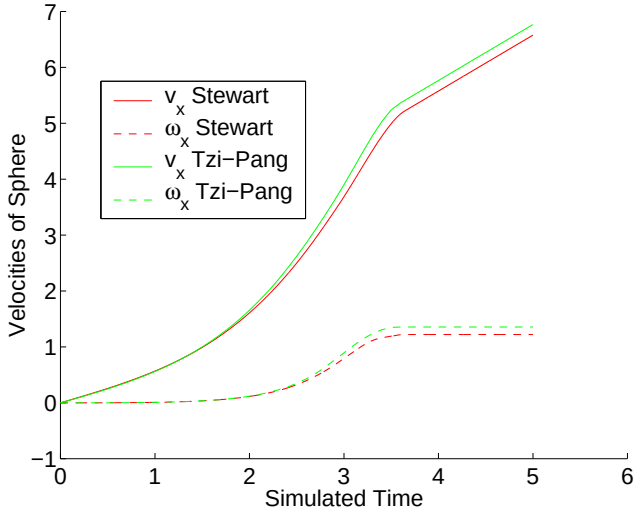

Figure 24: Selected Velocities: Stewart, $h = 0.0012$ and Tzitzouris-Pang, $h = 0.1$.

as Stewart did for the implicit version of his algorithm [12].

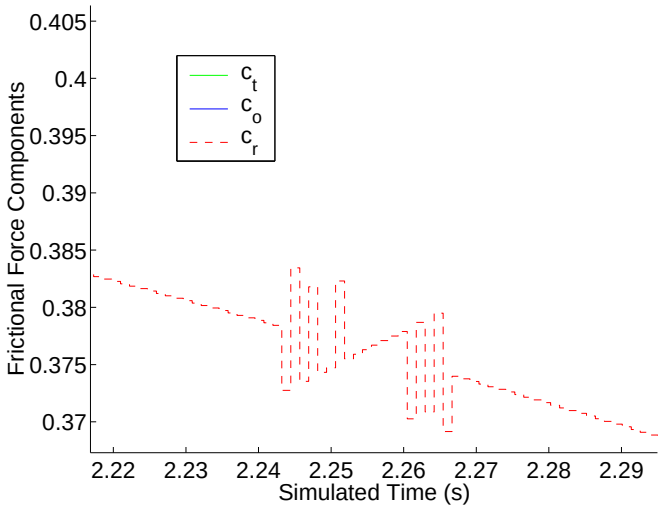

Figure 25: Chattering Phenomenon of c_r for $h = 0.0004$.

References

[1] G. Boothroyd and A.H. Redford. *Mechanized Assembly: Fundamentals of Parts Feeding, Orientation, and Mechanized Assembly*. McGraw-Hill, London 1968.

[2] D. Chan and J.S. Pang. The Generalized Quasi-Variational Inequality. *Mathematics of Operations Research*, **7**:211–222, 1982.

[3] P.W. Christensen and J.-S. Pang. *Reformulation – Nonsmooth, Piecewise Smooth, Semismooth and Smoothing Methods*, chapter Frictional contact algorithms based on semismooth Newton methods, pages 81–116. Kluwer Academic Publishers, 1999.

[4] R. W. Cottle, J.S. Pang, and R. E. Stone. *The Linear Complementarity Problem*. Academic Press, 1992.

[5] S. Goyal. *Planar Sliding of a Rigid Body with Dry Friction: Limit Surfaces and Dynamics of Motion*. PhD thesis, Cornell University Department of Mechanical Engineering, January 1989.

[6] R.D. Howe and M.R. Cutkosky. Practical Force-Motion Models for Sliding Manipulation. *International Journal of Robotics Research*, 1997.

[7] P. Lötstedt. Coulomb Friction in Two-Dimensional Rigid Body Systems. *Zeitschrift für Angewandte Mathematik und Mechanik*, **61**:605–615, 1981.

[8] J.-J. Moreau. Standard Inelastic Shocks and the Dynamics of Unilateral Constraints. In G. del Piero and F. Maceri, editors, *Unilateral Problems in Structural Mechanics*,

volume 288 of *C.I.S.M. Courses and Lectures*, pages 173–221, Vienna, New York, 1985. Springer-Verlag.

[9] J.S. Pang. Newton's Method for B-Differentiable Equations. *Mathematics of Operations Research* **15**:311–341, 1990.

[10] J.S. Pang and J.C. Trinkle. Complementarity Formulations and Existence of Solutions of Dynamic Multi-Rigid-Body Contact Problems with Coulomb Friction. *Mathematical Programming*, **73**:199–226, 1996.

[11] F. Pfeiffer and Ch. Glocker. *Multibody Dynamics with Unilateral Contacts*. Wiley, 1996.

[12] D.E. Stewart. Convergence of a Time-Stepping Scheme for Multi-Rigid-Body Dynamics and Resolution of Painlevé's Problems. *Archive Rational Mechanics Analysis*, **145**:215–260, 1998.

[13] D.E. Stewart and J.C. Trinkle. An Implicit Time-Stepping Scheme for Rigid Body Dynamics with Inelastic Collisions and Coulomb Friction. *International Journal of Numerical Methods in Engineering*, **39**:2673–2691, 1996.

[14] J.C. Trinkle and J.S. Pang. Dynamic Multi-Rigid-Body Systems with Concurrent Distributed Contacts. In *Proceedings, IEEE International Conference on Robotics and Automation*, pages 2276–2281, April 1997.

[15] J.C. Trinkle, J.S. Pang, S. Sudarsky, and G. Lo. On Dynamic Multi-Rigid-Body Contact Problems with Coulomb Friction. *Zeitschrift für Angewandte Mathematik und Mechanik*, **77**(4):267–279, 1997.

[16] J.C. Trinkle, J.A. Tzitzouris, and J.S. Pang. Dynamic Multi-Rigid-Body Systems with Concurrent Distributed Contacts: Theory and examples. Technical report, Sandia National Laboratories, Albuquerque, NM, 2001. forthcoming.

[17] J.A. Tzitzouris. Numerical Resolution of Multi-Rigid-Body Systems with Coulomb Friction, via Implicit Time-Stepping and Complementarity Methods. Ph.D. dissertation, Department of Mathematical Sciences, The Johns Hopkins University, in progress.

[18] J. A. Tzitzouris and J.-S. Pang. An Implicit High-Order Time-Stepping Scheme for Multi-Rigid-Body Systems with Coulomb Friction. *manuscript*, forthcoming.

Distribution:

Prof. Joris De Schutter
Katholieke Universiteit Leuven
Division PMA
Celestijnenlaan 300B
B-3001 Heverlee
Belgium

Prof. Dinesh K. Pai
Dept. of Computer Science
University of British Columbia
Vancouver, Canada

Prof. Xi Zexiang
Dept. of Electrical and
Electronic Engineering
Hong Kong University of Science
And Technology
Clear Water Bay, Kowloon
Hong Kong

Prof. Leo Joskowicz
Institute of Computer Science
The Hebrew University of Jerusalem
Jerusalem 91904, Israel

Prof. Makoto Kaneko
Dept. of Electrical and Electronics
Hiroshima University
1-4-1 Kagamlyama
Higashi-Hiroshima
Hiroshima 724 Japan

Prof. Tsuneo Yoshikawa
Dept. of Applied Systems Science
Faculty of Engineering
Kyoto University
Uji, Kyoto 611
Japan

Prof. Pierre DuPont
Dept. of Aerospace and
Mechanical Engineering
Boston University
Boston, MA 02215

Prof. Nancy S. Pollard
Dept. of Computer Science
Brown University
Box 1910
Providence, RI 02912

Prof. Joel Burdick
School of Engineering and
Applied Science
California Institute of
Technology
Pasadena, CA 91125

Prof. Mike Erdmann
School of Computer Science
Carnegie Mellon University
Pittsburgh, PA 15213-3890

Dr. Li Han
Institute for Complex Engineered
Systems (ICES)
Carnegie Mellon University
Pittsburgh, PA 15213-3890

Prof. Matthew Mason
School of Computer Science
Carnegie Mellon University
Pittsburgh, PA 15213

Prof. Wyatt Newman
EEAP Department
Case Western Reserve University
Cleveland, OH 44106

Prof. Peter Allen
Department of Computer Science
Columbia University
New York, NY 10027

Prof. Bruce Donald
Dartmouth
Computer Science
Hanover, NH

Prof. Jessica Hodgins
College of Computing
Georgia Institute of Technology
Atlanta, GA 30332

Prof. Rob Howe
Division of Applied Sciences
Pierce Hall, Rm. 321
Harvard University
Cambridge, MA 02138

Prof. David Stewart
Dept. of Mathematics
University of Iowa
Iowa City, IA 52242

Prof. Gregory S. Chirikjian
Dept. of Mechanical Engineering
Johns Hopkins University
Baltimore, MD 21218

Prof. Jong-Shi Pang
Department of Mathematical Sciences
Johns Hopkins University
Baltimore, MD 21218-2689

Prof. James A. Tzitzouris
Department of Mathematical Sciences
Johns Hopkins University
Baltimore, MD 21218-2689

Prof. Louis Whitcomb
Dept. of Mechanical Engineering
Johns Hopkins University
Baltimore, MD 21218

Prof. Joseph Schimels
Dept. of Mechanical Engineering
Marquette University
1515 Wisconsin Ave.
Milwaukee, WI 53233

Prof. Fue-Wen (Frank) Liou
Dept. of Mechanical and Aerospace Engineering
And Engineering Mechanics
Research Investigator of Intelligent Systems Center
University of Missouri-Rolla
Missouri's Technological University
121 ME Annex
Rolla, MO 65401-0249

Prof. John Hollerbach
Dept. of Biomedical Engineering
3775 University St.
McGill University
Montreal, Quebec H3A 2B4
Canada

Prof. Kevin Lynch
Laboratory for Intelligent Mechanical Systems
Dept. of Mechanical Engineering
Northwestern University
Evanston, IL 60208

Prof. Michael Peshkin
Mechanical Engineering Dept.
Northwestern University
Evanston, IL 60208

Dr. Jacob Barhen
Oak Ridge National Laboratory
P.O.Box 2008
Oak Ridge, TN 37831-6355

Prof. David Orin
Dept. of Electrical Engineering
Ohio State University
Columbus, OH 43210

Prof. Srinivas Akella
Dept. of Computer Science
Rennsaelaer Polytechnic Institute
Troy, NY 12180

Prof. Mark Cutkosky
Mechanical Engineering Dept.
Stanford University
Stanford, CA 94305

Prof. Imin Kao
Dept. of Mechanical Engineering
Suny at Stony Brook
Stony Brook, NY 11794-2300

Prof. Jim Bobrow
Dept. of Mechanical Engineering
University of California, Irvine
Irvine, CA 92697

Prof. John Canny
Computer Science Division
Department of EE and CS
University of California
Berkeley, CA 94720

Prof. Kenneth Goldberg
University of California
Industrial Eng. Oper. Research
4189 Etcheverry
Berkeley, CA 94720-1777

Prof. Mont Hubbard
Dept. of Mechanical Engineering
University of California
Davis, CA 95616

Prof. Michael McCarthy
Dept. of Mechanical Engineering
University of California
Irvine, CA 92717

Prof. Jean Ponce
Beckman Institute
University of Illinois
Urbana, IL 61801

Prof. Yu (Michael) Wang
G. L. Martin Institute of Technology
A. J. Clark School of Engineering
Dept. of Mechanical Engineering
University of Maryland
College Park, MD 20742

Prof. Raymond M. Brach
Dept. of Aerospace and Mechanical Engineering
University of Notre Dame
Notre Dame, IN 46556

Prof. Vijay Kumar
Dept. of Mechanical Engineering
And Applied Mechanics
University of Pennsylvania
Philadelphia, PA 19104

Dr. Brian Mirtich
MERL Cambridge Research
201 Broadway, 8th Floor
Cambridge, MA 02139

Chris Hecker
Definition Six
27A Embarcadero Cove
Oakland, CA 94606

Prof. A. E. Samuel
Robotics Laboratory
Dept. of Mechanical and
Manufacturing Engineering
The University of Melbourne
Parkville, Melbourne, Australia

Prof. Greg Starr
Dept. of Mechanical Engineering
University of New Mexico
Albuquerque, NM 87131

Prof. Jing Xiao
Computer Science Department
University or North Carolina
Charlotte
Charlotte, NC 28223

Prof. Blake Hannaford
Dept. of Electrical Engineering
University of Washington
Box 352500
Seattle, WA 98195-2500

Prof. Andy Ruina
Dept. of Theoretical and
Applied Mechanics
Cornell University
309 Kimball Hall
Ithaca, NY 14850

Prof. Florian Potra
Dept. of Mathematics and
Statistics
University of Maryland
Baltimore County
1000 Hilltop Circle
Baltimore, MD 21250

Prof. Elisha Sacks
Dept. of Computer Science
Purdue University
West Lafayette, IN 47907

Prof. Yildirim Hurmuluz
Dept. of Mechanical Engineering
Southern Methodist University
P.O. Box 750337
Dallas, TX 75275

Prof. Wes Huang
Dept. of Computer Science
Rennsaelaer Polytechnic Institute
Troy, NY 12180

Prof. Richard Cottle
Dept. of Engineering – Economic
Systems and Operations Research
Stanford University
Terman Engineering Center, Rm 411
Stanford, CA 94305-4026

Prof. Kalyan Chatterjee
Dept. of Management Science
The Pennsylvania State University
University Park, PA 16802

Prof. Antonio Bicchi
Interdept. Research Center “Enrico
Piaggio”
Universita’ di Pisa
Via Diotisalvi, 2
56125 Pisa
Italy

MS 1004 Center Library (5)
MS 1002 P. J. Eicker, 15200
MS 1004 R. W. Harrigan, 15221
MS 1004 J. C. Trinkle, 15221
MS 1125 M. R. Vaughn, 15252
MS 9018 Central Technical Files, 8945-1
MS 0899 Technical Library, 9616
MS 0612 Review & Approval Desk, 9612
For DOE/OSTI
MS 0161 Patent & Licensing, 11500